Journal of The Electrochemical Society, **157** (7) H750-H754 (2010)
0013-4651/2010/157(7)/H750/5/$28.00 © The Electrochemical Society

The Electromechanical Characteristics of ZnO Grown on Poly(ethylene terephthalate) Substrates

Hao-Huai Shieh,[a] I-Chun Cheng,[a,z] Jian Z. Chen,[b,*,z] Chun-Ching Hsiao,[b,c] Pei-Chun Lin,[d] and Yung-Hui Yeh[e]

[a]Department of Electrical Engineering and Graduate Institute of Photonics and Optoelectronics, [b]Institute of Applied Mechanics, [c]Nano-Electro-Mechanical-Systems Research Center, and [d]Department of Mechanical Engineering, National Taiwan University, Taipei 10617, Taiwan
[e]Electronics and Optoelectronics Research Laboratory, Industrial Technology Research Institute, Hsinchu County 31040, Taiwan

We investigate the electromechanical properties of ZnO grown on poly(ethylene terephthalate) (PET) and compare the results with those obtained from the counterparts on glass substrates. The elastic moduli of ZnO on PET (measured by a microstretcher) are very close to those of ZnO grown on glass substrates (measured by nanoindentation): The moduli decrease then increase as the O_2/Ar ratio increases. Films start to peel off from the plastic substrates when oxygen content reaches 50%. The in situ measurement of the ZnO resistance under uniaxial tensile stretching is influenced by the induced piezoelectric voltage, leading to a reduction in the electrical resistance for highly resistive ZnO films. The trend of the preferred orientation in relation to the oxygen content of the sputtering atmosphere is the same for ZnO films grown on either PET or glass substrates. The optical bandgap (E_g) of the ZnO films on both substrates exhibits crystal orientation dependence, varying from 3.18 eV with (002) preferred orientation to 3.25 eV, with a large number of (100) and (101) oriented crystals.

[DOI: 10.1149/1.3428416]

Manuscript submitted November 9, 2009; revised manuscript received April 16, 2010. Published May 18, 2010.

Flexible electronics attracts much attention due to its versatile application, such as E-papers, cell phones, and roll up portable displays. One requisite core technology is the fabrication of electronic components or systems on compliant substrates so that they can function while flexing. Recent experiments have focused on the implementation of optoelectronic materials, such as amorphous/nanocrystalline silicon,[1,2] organic semiconductor materials,[3] and transparent semiconducting oxides,[4] onto compliant substrates. Hydrogenated amorphous silicon technology is so far the industrial standard technology for large-area electronics. However, its electron mobility is limited up to 1 $cm^2 V^{-1} s^{-1}$.[5] As a result, many research efforts have been made on investigating large-area transition-metal oxide semiconductors to realize electronics with higher carrier mobility.[4,6]

ZnO is a representative transparent semiconducting oxide[7] and has been applied in a variety of devices, such as solar cells, thin-film gas sensors, transparent thin-film transistors, transparent conductive contacts, UV lasers, and luminescent devices.[8-11] There are various techniques for preparing ZnO films, such as sputtering,[12] pulsed laser deposition (PLD),[13] molecular beam epitaxy,[14] metallorganic chemical vapor deposition,[15] and spray pyrolysis.[16] Among these methods, magnetron sputtering shows promise for large-area deposition because of its low cost, scalability, and ability to grow materials on substrates with low melting points.[17] ZnO films grown on rigid substrates by these fabrication methods exhibit a strong (002) preferred orientation and are strongly affected by the oxygen content in the sputtering atmosphere during film deposition.[18-22]

In flexible electronics, the rigid substrate is replaced with the compliant foil substrate. Therefore, the mechanics of the thin-film-on-foil-substrate must be considered in addition to the electrical performance of the electronic devices. Mechanical stress may arise during the fabrication, such as residual stress from the thin-film deposition process or intentional tensile stress applied during the roll-to-roll process.[6] In addition, the electronic devices may be operated under mechanical flexing, which may render the alteration in device performance.[4,23,24] Therefore, it is important to understand the interdependence between the mechanical and electrical properties of the thin-film-on-foil-substrate system.

In this study, we correlate not only the electronic properties but also the mechanical properties of ZnO films with the parameters of the sputtering process. The influence of sputtering oxygen partial pressure (the ratio of oxygen to argon, O_2/Ar) on the microstructural, electromechanical, and optical properties of ZnO grown on poly(ethylene terephthalate) (PET) is studied and the results are compared with ZnO grown on glass substrates under the same deposition condition. The experimental results can provide useful information for ZnO-based flexible electronics. The elastic moduli of ZnO on plastic substrates (measured with a custom microstretcher) are compared with those of a ZnO film on glass substrates (measured by a nanoindentation system). The electrical properties of ZnO thin films on plastic are also characterized under stretching. Upon stretching, different transition trends of the electrical behavior are found for the ZnO films grown under a different oxygen content. Other properties of ZnO grown on PET and on glass substrates are also compared and discussed.

Experimental

ZnO thin films were deposited on 50 μm thick PET (CH 185E from NAN YA) and 0.7 mm thick glass substrates (EAGLE 2000 from Corning). All substrates were cleaned in a detergent (micro-90) bath at 80°C, followed by rinsing with deionized water. The ZnO films were radio-frequency (rf) sputter-deposited from a ZnO target (99.95%, GFE). Before the sputtering deposition, the chamber was pumped to a base pressure of 8×10^{-6} Torr. The sputtering deposition was performed with a sputtering power of 100 W at an O_2/Ar mixture atmosphere of 5 mTorr, in which the O_2/Ar ratio was varied from 0/1, 1/9, 1/6, 1/3, to 1/1. To balance the stress-induced curvature and maintain the flatness of the PET samples after ZnO deposition, we intentionally stepwise two-side coated the PET strips using the same deposition condition. The ZnO films adhered well to glass and PET substrates under all sputtering conditions, except for the films deposited in an O_2/Ar atmosphere of 1/1, where the films peeled off from the PET substrates.

The crystal structures were characterized using an X-ray diffractometer (XRD, X'Pert PRO) with Cu Kα radiation (λ = 0.15406 nm). A scanning electron microscope (SEM, Hitachi S-800) and an atomic force microscope (AFM, OBJ-204C) were used for surface morphology inspection. The elastic moduli of ZnO films on glass substrates were measured with a nanoindentation system (TI 900 TriboIndenter, Hysitron Inc.). In this experiment, we deposited the films for 12 h to obtain ZnO films thicker than 900 nm to avoid the contacts between the nanoindenter with the solid glass substrates during the indentation procedure. The elastic moduli of ZnO films on PET were determined from the stress–strain curves

---

[*] Electrochemical Society Active Member.
[z] E-mail: ichuncheng@cc.ee.ntu.edu.tw; jchen@ntu.edu.tw

obtained with a microstretcher. The stretching rate was set to be 1 μm/s. After the sample was stretched to each specific strain, the movement of the fixtures of the microstretcher was stopped and the resistance was measured as a function of the applied strain using a Keithley 2636A sourcemeter. The optical transmittances were measured using a JASCO V-570 ultraviolet-visible (UV-vis) near-IR spectrophotometer to determine the optical bandgaps.

Results and Discussion

Crystalline microstructure.— Figure 1 shows the XRD results for the sputtered ZnO films on glass (Fig. 1a) and PET substrates (Fig. 1b). In both cases the preferred orientations change from a combination of (100) and (101) to (002) as the O_2/Ar ratio increases from 0 to 1/9–1/6. A further increase in O_2/Ar during sputtering suppresses the (002) preferred orientation, and (100) and (101) crystal orientations reoccur. This transition of crystalline orientation is the same for ZnO films deposited on either glass or PET substrates. Other groups also observe similar experimental phenomena when depositing films on rigid substrates, such as Si wafer, glass, and quartz.[18,19,21] This suggests that the crystalline orientations of sputtered ZnO films are influenced more by the sputtering atmosphere than by the substrate type. By detecting the glow discharge spectra of the plasma during a ZnO rf sputtering process, Aita et al. found that the crystallographic orientation transition is highly correlated with the ratio of Zn to ZnO ions in the plasma.[18] Gu et al. discovered an enhancement of the ZnO (002) preferred orientation while adding plasma oxygen during PLD, but the enhancement of (002) orientation is not significant when gaseous oxygen is added during the deposition.[22]

Based upon the full width half-maximum (fwhm) and positions of the (002) diffraction peaks, we can calculate the grain sizes and the residual stresses in the films. The average grain size D in the film is calculated by the Scherrer formula[19]

$$D = \frac{0.9\lambda}{\beta \cos \theta} \tag{1}$$

where λ is the radiation wavelength, θ is the Bragg angle of the (002) peak, and β is the fwhm value. The residual stresses parallel to the substrate were calculated based on the biaxial stress model formula[25,26]

$$\sigma_{\text{film}} = \left(\frac{2C_{13}^2 - C_{33}(C_{11} + C_{12})}{C_{13}}\right) \times \varepsilon_{\text{film}} \tag{2}$$

where C_{ij} are the elastic constants and $\varepsilon_{\text{film}} = \Delta d_{002}/d_{002}$. The corresponding values of single-crystal ZnO used were $C_{11} = 208.8$, $C_{33} = 213.8$, $C_{12} = 119.7$, $C_{13} = 104.2$ GPa, and $d_{002} = 0.26033$ nm. With all these constants substituted, Eq. 2 is simplified to

$$\sigma_{\text{film}} = -465(\Delta d_{002}/d_{002}) \text{ GPa} \tag{3}$$

Figures 1c and d show plots of residue stresses and grain sizes as a function of O_2/Ar during sputtering. Under all of our sputtering conditions, the residual stresses of deposited ZnO films are compressive. The vertical dimension of grains, whose (002) basal plains are parallel to the substrates, decreases with an increase in the oxygen partial pressure during the sputtering deposition, but the variation is very small.

Surface morphology.— Figures 2a-e show the SEM images of the glass substrates. For various oxygen partial pressures, the surface morphology is quite different for the deposited ZnO films. Large surface grain dimensions are shown on the films deposited with O_2/Ar ratio. The insets in each figure show AFM images measured over a 5 × 5 μm square. The surface roughness is measured and plotted in Fig. 2f from each AFM image. The surface roughness increases from ~74 to ~90 nm as the O_2/Ar ratio increases from 0/1 to 1/1 during sputtering deposition.

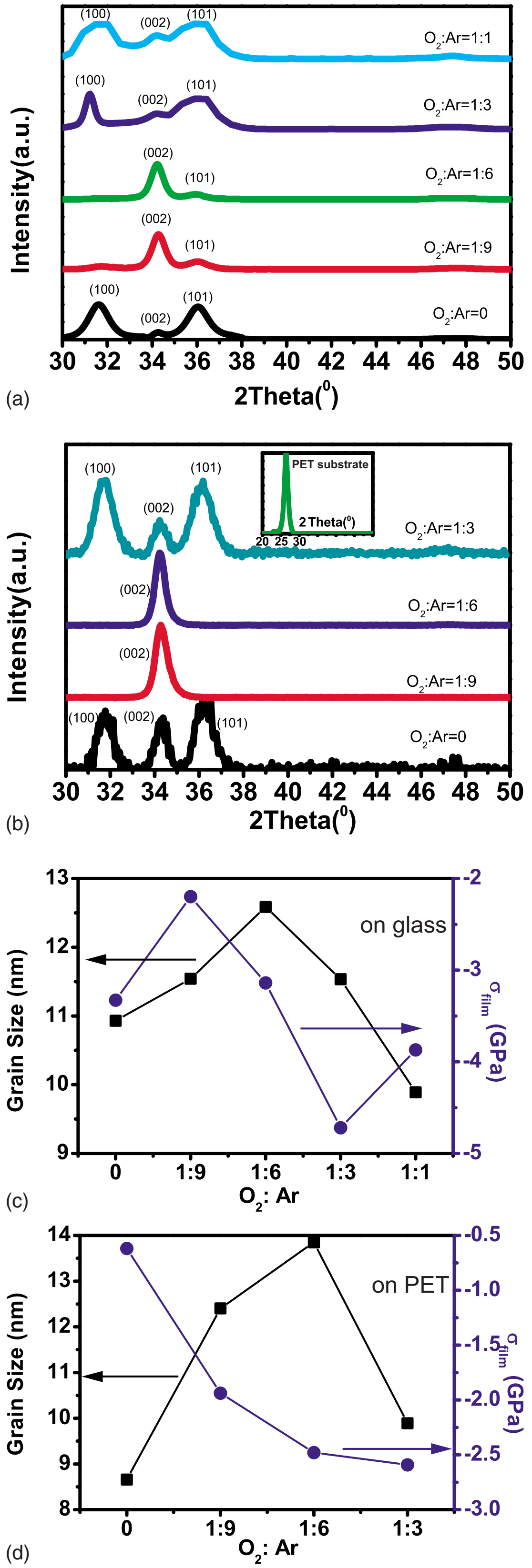

Figure 1. (Color online) [(a) and (b)] XRD patterns of (a) ZnO films on glass substrates and (b) ZnO films on PET substrates. Inset of (b): XRD peak from a PET substrate. [(c) and (d)] Grain sizes and residue stresses σ_{film} calculated from the ZnO(002) diffraction peak. (c) ZnO films on glass substrates. (d) ZnO films on PET substrates.

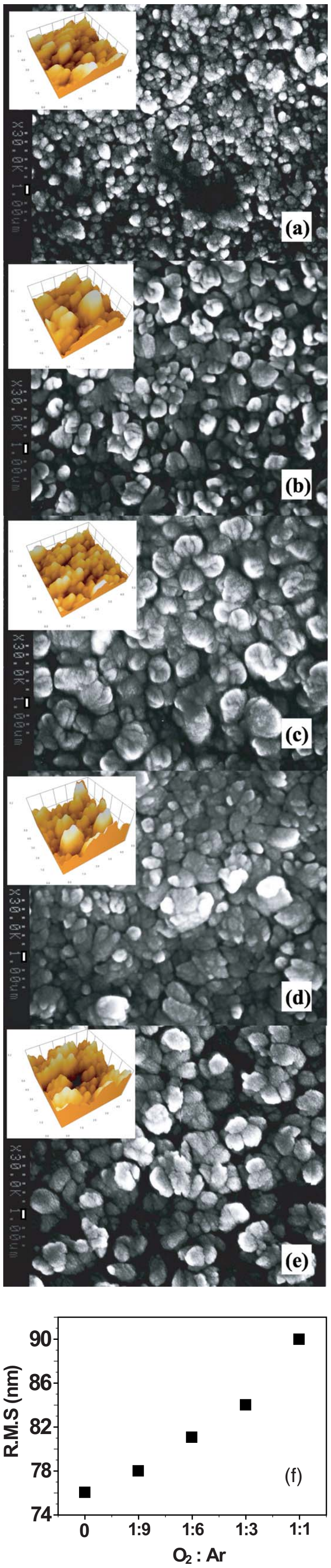

Figure 2. (Color online) SEM images of ZnO films on glass substrates. (a) $O_2/Ar = 0/1$, (b) $O_2/Ar = 1/9$, (c) $O_2/Ar = 1/6$, (d) $O_2/Ar = 1/3$, and (e) $O_2/Ar = 1/1$. Insets: The corresponding AFM images measured over a 5×5 μm square. (f) The surface roughness of ZnO films measured by AFM.

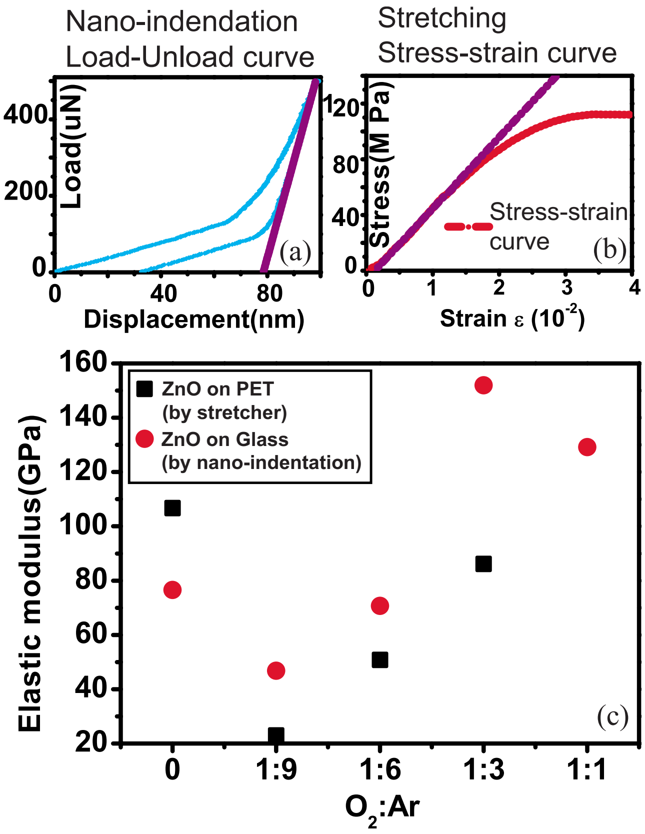

Figure 3. (Color online) (a) Nanoindentation of the load–unload curve. (b) Microstretching stress–strain curve. (c) Comparison of elastic moduli measured from nanoindentation and the microstretcher.

Mechanical property.— The elastic moduli of the ZnO films on glass are characterized using nanoindentation. We calculate the elastic modulus of the ZnO film deposited on glass using two equations[27]

$$E_r = \frac{1}{\beta_1}\frac{\sqrt{\pi}}{2}\frac{S}{\sqrt{A}} \qquad [4]$$

where E_r is the reduced elastic modulus, β_1 is the geometric constant that depends on the indenter, $S = dP/dh$ is the elastic contact stiffness calculated from the slope of the unloading curve in the plot of load–displacement (see Fig. 3a), and A is the projected contact area at the peak. With Berkovich indenters, β_1 is 1.034. The elastic modulus of ZnO film can be determined by

$$\frac{1}{E_r} = \frac{1-\nu^2}{E} + \frac{1-\nu_i^2}{E_i} \qquad [5]$$

where E (E_i) and ν (ν_i) are the elastic modulus and Poisson's ratio, respectively, of the film (the indenter). E_i and ν_i are 1141 GPa and 0.07, respectively, for a diamond indenter. ν is 0.3 and E is the ZnO elastic modulus to be determined.

The elastic modulus of the film grown on a PET substrate is determined from the stress–strain curve using the uniaxial tensile stretching experiment. Using the following equations, we can calculate the elastic modulus

$$\sigma = E_{tot}\varepsilon \qquad [6]$$

$$E_f = \frac{E_{tot}(t_s + t_f) - E_s t_s}{t_f} \qquad [7]$$

where σ is the tensile stress, ε is the strain, and E_{tot} is the elastic modulus of the whole film–plastic substrate system, which is deter-

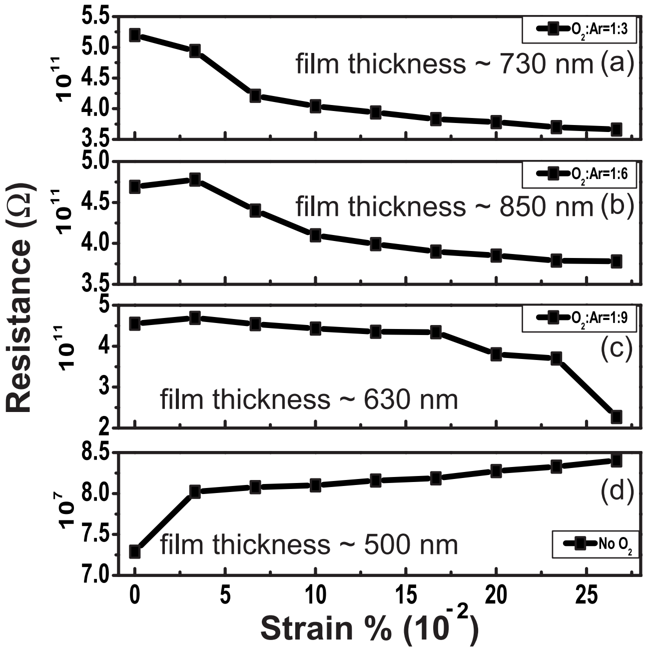

Figure 4. ZnO film resistance changes with applied strain using the microstretcher for (a) $O_2/Ar = 1/3$, (b) $O_2/Ar = 1/6$, (c) $O_2/Ar = 1/9$, and (d) $O_2/Ar = 0/1$.

mined from the slope of the tangential line for the stress–strain curve, as illustrated in Fig. 3b. E_f (E_s) is the elastic modulus of the film (substrate) and t_f (t_s) is the film (substrate) thickness.

The comparison of the elastic moduli of ZnO on glass (measured by nanoindentation) and ZnO on PET (measured with a microstretcher) is plotted as a function of the sputtering oxygen content, as shown in Fig. 3c. The relationship between the elastic modulus of the ZnO films and the sputtering oxygen content exhibits a similar trend in both measurements, although the overall measured elastic moduli of ZnO on PET substrates are smaller. The measured elastic moduli of sputtered ZnO range from ∼20 to ∼160 GPa. The elastic moduli are smallest (∼20 to 60 GPa) when ZnO exhibits a (002) preferred orientation. The elastic modulus seems to correlate to the crystal orientation. With more grains with the (002) basal plane parallel to the substrate, the elastic modulus is smaller. In this regard, the dependence of the measured elastic modulus on the crystal orientation is misleading because the elastic property of wurtzite ZnO is very close to isotropy due to its symmetry.[26] This elastic modulus dependence on the preferred thin-film texture is likely due to changes in the material microstructure and defects created by ion bombardment in the deposited films as the sputtering oxygen content varies.[15,21] Ong et al. used the microbridge method to measure ZnO films sputtered at a substrate temperature of 400°C under an O_2/Ar ratio of 7/3. The measured elastic modulus is ∼137 GPa,[28] close to that of our experimental film deposited with a high oxygen content. Other groups measured the elastic moduli of bulk ZnO to be ∼140 to ∼144 GPa using acoustic wave methods[29] and ∼111 GPa by a nanoindentation method.[30]

Electrical property under uniaxial tensile stress.— Figures 4a-d show the resistance of ZnO on PET (measured in the tensile direction) under uniaxial tensile stress. The ZnO films deposited with the addition of oxygen (see Fig. 4a-c) in a sputtering atmosphere exhibit greater electrical resistivity ($\sim 10^7$ Ω cm) than those deposited in pure argon ($\sim 10^3$ Ω cm) (see Fig. 4d), owing to the lack of oxygen vacancies and Zn interstitials.[31] This resistivity difference could be caused by the oxygen ions in the plasma rather than oxygen molecules because the resistivity of ZnO deposited by PLD increases when plasma oxygen is added during the process, whereas the resistivity remains relatively small when gaseous oxygen is added.[22]

The resistance of the ZnO films deposited in pure argon increases with an increase in applied strain (see Fig. 4d), but the resistance–strain curve shape is different from the typical ones for ZnO:Al ($\rho \sim 10^{-3}$ Ω cm) on plastic.[32] The ZnO films deposited with oxygen in the sputtering atmosphere show high resistance, which decreases with the applied strain (see Fig. 4a-c). This may result from the piezoelectric nature of ZnO.[33] When ZnO is subjected to deformation during electrical measurements, a piezoelectric voltage is added to the externally applied voltage. This modifies the measured current, thus the measured resistance values. For ZnO:Al ($\rho \sim 10^{-3}$ Ω cm),[32] the measured current is completely dominated by the externally applied voltage and the resistance is determined by the ZnO:Al film geometry. In our relatively high conducting ZnO ($\rho \sim 10^3$ Ω cm, deposited under an atmosphere without oxygen), the piezoelectric voltage induced by tensile stress modifies the measured current slightly; thus, the resistance increases with the applied strain, similar to a stretched conductor. For highly resistive ZnO ($\rho \sim 10^7$ Ω cm, deposited under an atmosphere with oxygen added), the current induced by the piezoelectric voltage during strain is comparable to that of the externally applied voltage during electrical measurement, leading to a decrease in resistance with increasing applied strain.

Optical properties.— Figures 5a and b show the transmittance spectra for ZnO grown on PET and glass substrates. The transmittance reaches ∼80% in the visible region. From the Tauc model in the high absorbance region, the relation between incident photons and optical bandgap E_g is[34]

$$\alpha h\nu = A(h\nu - E_g)^{1/2} \qquad [8]$$

where α is the absorption coefficient, $h\nu$ is the photon energy, E_g is the optical bandgap, and A is a constant. From the transmittance plot, we can calculate the absorption coefficient α

$$T = B \cdot \exp(-\alpha d) \qquad [9]$$

where T is the transmittance of the film, B is a constant which is close to unity, and d is the film thickness. Plotting $(\alpha h\nu)^2$ against $h\nu$, E_g can be obtained from the x-intercept of the tangential line. The comparison of E_g for the ZnO films grown on glass and PET is plotted in Fig. 5c. E_g is larger overall for the ZnO films sputtered on PET than on glass substrates. In both cases, E_g is smaller as the ZnO films exhibit a (002) preferred orientation; yet E_g becomes larger as the ZnO films reveal (100) and (101) preferred orientation textures.

Conclusion

We investigate the influence of the sputtered atmosphere of O_2/Ar ratio on the microstructural, optical, and electromechanical properties of ZnO films grown on PET and glass. Oxygen influences ZnO grown on either PET or glass substrates in a similar fashion. The preferred crystal orientation of ZnO films is strongly influenced by the O_2/Ar ratio. ZnO films exhibit a preferred crystal orientation of (100) and (101) parallel to the substrates when deposited with $O_2/Ar = 0/1$. As the O_2/Ar increased to 1/9 and 1/6, the films show highly ordered crystal orientation with the (002) plane, parallel to the substrate surfaces. Further increasing O_2/Ar diminishes the strong (002) preferred orientation. The elastic modulus of the ZnO film also depends on the sputtering atmosphere. The elastic modulus is smallest (∼20 to 60 GPa) when ZnO is deposited at $O_2/Ar = 1/9$ and 1/6, owing to the defects in materials induced by ion bombardment. The ZnO films sputtered without any oxygen reveal a resistivity of about 4 orders of magnitude smaller than those sputtered with oxygen content. The resistance of the ZnO film sputtered in an oxygen-free atmosphere increases as the amount of strain increases, yet ZnO sputtered with oxygen content shows the opposite trend as the applied strain increases. This is caused by the induced piezoelectric voltage during deformation. The optical bandgap E_g

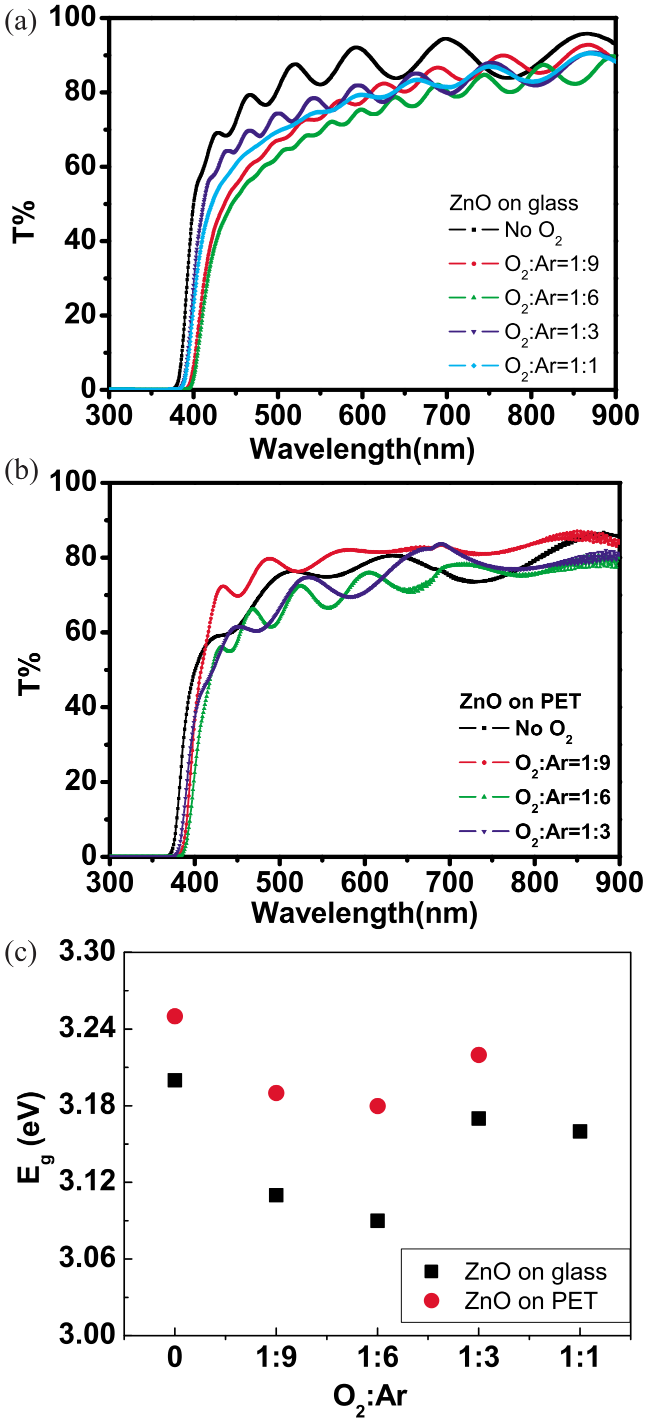

Figure 5. (Color online) UV-vis transmittance of (a) ZnO film on glass, (b) ZnO film on PET, and (c) comparison of optical bandgap E_g for ZnO grown on glass and PET.

also exhibits a crystal orientation dependence. E_g is, in general, smaller for ZnO sputtered on glass substrates than that sputtered on PET substrates. E_g varies from 3.18 eV [when films exhibit a (002) preferred orientation] to 3.25 eV [when films show a large amount of (100) and (101) oriented crystals].

Acknowledgment

I.C.C. and J.Z.C. gratefully acknowledge the funding support from the National Science Council of Taiwan, under grant no. NSC 97-2221-E-002-236, no. NSC 98-3114-E-002-001, and no. NSC 98-2120-M-002-005 (I.C.C.); no. NSC 97-2221-E-002-052 and no. NSC 98-2221-E-002-169 (J.Z.C.), as well as the early stage funding from the Electronics and Optoelectronics Research Laboratory, Industrial Technology Research Institute, Taiwan.

National Taiwan University assisted in meeting the publication costs of this article.

References

1. K. Long, A. Z. Kattamis, I.-C. Cheng, H. Gleskova, S. Wagner, and J. C. Sturm, *IEEE Electron Device Lett.*, **27**, 111 (2006).
2. J. H. Cheon, W. G. Lee, T. H. Lim, and J. Jang, *Electrochem. Solid-State Lett.*, **12**, J25 (2009).
3. T. W. Kelley, P. F. Baude, C. Gerlach, D. E. Ender, D. Muyres, M. A. Haase, D. E. Vogel, and S. D. Theiss, *Chem. Mater.*, **16**, 4413 (2004).
4. K. Nomura, H. Ohta, A. Takagi, T. Kamiya, M. Hirano, and H. Hosono, *Nature (London)*, **432**, 488 (2004).
5. I.-C. Cheng and S. Wagner, *Appl. Phys. Lett.*, **80**, 440 (2002).
6. W. B. Jackson, in *Flexible Electronics: Materials and Applications*, W. S. Wong and A. Salleo, Editors, p. 107, Springer, New York (2009).
7. Ü. Özgür, Y. I. Alivov, C. Liu, A. Teke, M. A. Reshchikov, S. Dogan, V. Avrutin, S.-J. Cho, and H. Morkoç, *J. Appl. Phys.*, **98**, 041301 (2005).
8. W. W. Wenas, A. Yamada, K. Takahashi, M. Yoshino, and M. Konagai, *J. Appl. Phys.*, **70**, 7119 (1991).
9. H. Ohta, K. Kawamura, M. Orita, M. Hirano, N. Sarukura, and H. Hosono, *Appl. Phys. Lett.*, **77**, 475 (2000).
10. H. S. Kang, J. S. Kang, J. W. Kim, and S. Y. Lee, *J. Appl. Phys.*, **95**, 1246 (2004).
11. R. Navamathavan, E. J. Yang, J. H. Lim, D. K. Hwang, J. Y. Oh, J. H. Yang, J. H. Jang, and S. J. Park, *J. Electrochem. Soc.*, **153**, G385 (2006).
12. A. V. Singh, R. M. Mehra, A. Wakahara, and A. Yoshida, *J. Appl. Phys.*, **93**, 396 (2003).
13. X. W. Sun and H. S. Kwok, *J. Appl. Phys.*, **86**, 408 (1999).
14. K. Nakahara, H. Takasu, P. Fons, A. Yamada, K. Iwata, K. Matsubara, R. Hunger, and S. Niki, *J. Cryst. Growth*, **237–239**, 503 (2002).
15. B. P. Zhang, K. Wakatsuki, N. T. Binh, N. Usami, and Y. Segawa, *Thin Solid Films*, **449**, 12 (2004).
16. J.-L. Zhao, X.-M. Bian, W.-D. Yu, and C.-Y. Zhang, *J. Cryst. Growth*, **280**, 495 (2005).
17. K. Ellmer, *J. Phys. D*, **33**, R17 (2000).
18. C. R. Aita, A. J. Purdes, R. J. Lad, and P. D. Funkenbusch, *J. Appl. Phys.*, **51**, 5533 (1980).
19. R. Hong, H. Qi, J. Huang, H. He, Z. Fan, and J. Shao, *Thin Solid Films*, **473**, 58 (2005).
20. J. P. Zhang, G. He, L. Q. Zhu, M. Liu, S. S. Pan, and L. D. Zhang, *Appl. Surf. Sci.*, **253**, 9414 (2007).
21. S. H. Jeong, B. S. Kim, and B. T. Lee, *Appl. Phys. Lett.*, **82**, 2625 (2003).
22. Y. Gu, X. Li, W. Yu, X. Gao, J. Zhao, and C. Yang, *J. Cryst. Growth*, **305**, 36 (2007).
23. I.-C. Chiu, J.-J. Huang, Y.-P. Chen, I.-C. Cheng, J. Z. Chen, and M.-H. Lee, *IEEE Electron Device Lett.*, **57**, 696 (2010).
24. J. Z. Chen, C.-Y. Yeh, I.-C. Chiu, I.-C. Cheng, J.-J. Huang, and Y.-P. Chen, *Mater. Res. Soc. Symp. Proc.*, **1153**, A20-02 (2009).
25. K. C. Ruthe and S. A. Barnett, *Surf. Sci. Lett.*, **538**, L460 (2003).
26. Y. F. Li, B. Yao, Y. M. Lu, Y. Q. Gai, C. X. Cong, Z. Z. Zhang, D. X. Zhao, J. Y. Zhang, B. H. Li, D. Z. Shen, et al., *J. Appl. Phys.*, **104**, 083516 (2008).
27. W. C. Oliver and G. M. Pharr, *J. Mater. Res.*, **7**, 1564 (1992).
28. C. W. Ong, D. G. Zong, M. Aravind, C. L. Choy, and D. R. Lu, *J. Mater. Res.*, **18**, 2464 (2003).
29. T. B. Bateman, *J. Appl. Phys.*, **33**, 3309 (1962); T. Azuhata, M. Takesada, T. Yagi, A. Shikanai, S. F. Chichibu, K. Torii, A. Nakamura, T. Sota, G. Cantwell, D. B. Eason, et al., *J. Appl. Phys.*, **94**, 968 (2003).
30. S. O. Kucheyev, J. E. Bradby, J. S. Williams, C. Jagadish, and M. V. Swain, *Appl. Phys. Lett.*, **80**, 956 (2002).
31. L. Schmidt-Mende and J. L. MacManus-Driscoll, *Mater. Today*, **10**, 40 (2007).
32. E. Fortunato, P. Nunes, A. Marques, D. Costa, H. Águas, I. Ferreira, M. E. V. da Costa, M. H. Godinho, P. L. Almeida, J. P. Borges, et al., *Adv. Eng. Mater.*, **4**, 610 (2002).
33. A. R. Hutson, *Phys. Rev. Lett.*, **4**, 505 (1960).
34. S. T. Tan, B. J. Chen, X. W. Sun, X. Hu, X. H. Zhang, and S. J. Chua, *J. Cryst. Growth*, **281**, 571 (2005).